



1 Article

Structural Characterization of Nanocellulose/Fe3O4 Hybrid Na-

3 nomaterials

- 4 Aleksandra Janićijevic 1, Vera P. Pavlovic 2, Danijela Kovacevic 1, Marko Peric 3, Branislav Vlahovic 4,5, Vladimir B.
- 5 Pavlovic 6,* and Suzana Filipovic 7
- 6 7 8 9 10 11 12 13 14
- 17 18 19 20
- 23 24 25 26 27 28

22

- Citation: Lastname, F.; Lastname, F.; Lastname, F. 3:0
 Lastname, F. Title. *Polymers* 2022, 14, x. https://doi.org/10.3390/xxxxx

 Academic Editor: Firstname Last- 32
- name 33
 Received: date 34
 Accepted: date

Published: date

Publisher's Note: MDPI stays neutral with regard to jurisdictional claims in published maps and institu^{3,7} tional affiliations.



Copyright: © 2022 by the authors. Submitted for possible open access publication under the terms and conditions of the Creative Commons. Attribution (CC BY) license (https://creativecommons.org/license s/by/4.0/).

- Academy of Applied Technical Studies Belgrade, Katarine Ambrozic 3, 11000 Belgrade, Serbia; ajanici-jevic@politehnika.edu.rs (A.J.); dkovacevic@politehnika.edu.rs (D.K.)
- 2 University of Belgrade, Faculty of Mechanical Engineering, Kraljice Marije 16, 11000 Belgrade, Serbia; verapetarpavlovic@gmail.com
- 3 University of Belgrade, Vinca Institute of Nuclear Sciences, National Institute of the Republic of Serbia, Mike Petrovica Alasa 12-14, 11000 Belgrade, Serbia; markoperic1983@gmail.com
- 4 North Carolina Central University, Durham, NC 27707, USA; vlahovic@nccu.edu
- 5 NASA University Research Center for Aerospace Device Research and Education and NSF Center of Research Excellence in Science and Technology Computational Center for Fundamental and Applied Science and Education, Durham, NC 27707, USA
- 6 University of Belgrade, Faculty of Agriculture, Department for Physics and Mathematics, Nemanjina 6, Zemun, 11000 Belgrade, Serbia
- 7 Institute of Technical Sciences of SASA, Knez Mihailova 35/IV, 11000 Belgrade, Serbia; suzana.fil-ipovic@itn.sanu.ac.rs
- * Correspondence: vladimirvboskopavlovic@gmail.com

Abstract: The rise of innovation in the electrical industry is driven by the controlled design of new materials. The hybrid materials based on magnetite/nanocellulose are highly interesting due to their various applications in medicine, ecology, catalysis and electronics. In this study, the structure and morphology of nanocellulose/magnetite hybrid nanomaterials were investigated. The effect of nanocellulose loading on crystal structure of synthesized composites was investigated by XRD and FTIR methods. The presented study revealed that the interaction between the cellulose and magnetic nanoparticles depends on nanocellulose content. Further, transition from cellulose II to cellulose I allomorph was observed. SEM and EDS were employed to determine variation in morphology with changes in component concentrations. By calculation of magnetic interactions between adjacent Fe³⁺ and Fe²⁺ ions within composites, it was determined that ferromagnetic coupling predominates

Keywords: Nanocomposites; Polymer synthesis; Nanocellulose; Fe₃O₄ functionalization; DFT calculation

1. Introduction

Development of hybrid organic/inorganic composites attracts great attention in the scientific community. Hybrid multifunctional materials have advantages, due to combination of different properties of organic-inorganic ingredients, where an organic component, such as nanocellulose, contributes with high flexibility, dielectric and piezoelectric properties, while inorganic component may contribute in magnetic and electric properties [1]. Several studies emphasized the importance of achieving improved material properties through the prevention of mutual inhibition of different origin fillers and promotion of compatibility at the interface matrix/added components. Resulting hybrid material have shown diverse properties, which can be tailored by changing components, loadings, morphology, the arrangement of an individual component, etc. [2, 3]. As a result, the ma-

60 61

62

63

65

67

69

70

71

72 73

74

76

77

78

81

83

84

86

87

88

90

92

93

94

95

97

terials with a broad range of applications, such as drug delivery, magnetic resonance imaging (MRI), sensors, magnetic storage media, photocatalysts, electromagnetic absorption materials etc., can be developed [4–9].

A biosensors are devices which convert (bio)chemical information into an electronic signal by an appropriate transducer containing a analyte detection structures. Such measured signal can be read by an instrument. The major problems for modern biosensors low reproducibility and the lower stability of the bioreceptor. Thus, cellulose-based materials possess fine fibrous matrix that is convinient for immobilizing receptor or nanoparticles, metal oxides and enzymes [10,11].

Nanocellulose (NC) is one of the most frequently used biomass in nature, because NC is easily degradable, renewable, non-toxic, posses high reinforcing strength, stiffness and is low-cost material [12]. It should be noticed that NC and its composites are far more used as a barrier for liquid and gaseous materials, biomedicine, catalysis and water purification [13-15]than for electronic or multiferroic applications, despite their good dielectric and piezoelectric properties [16, 17].

The main disadvantages of NC for these types of applications are related to its polar and hydrophilic nature owing to the existence of -OH groups on their surface, which can be avoided by surface modification [18, 19]. As a result, controlled modification of nanocellulose surface offers the possibility for the production of electronic hybrid inorganic-organic nanomaterials. For this type of investigation, nanocellulose has been coated with various magnetic particles [20-24]. It has been found that incorporation of magnetite into NC enables selectively targeting, detection, and potentially treatment of the cancer tissue via magnetic resonance imaging and inductive heating. This approach can be applied in the biomedical area, for sensors, etc., due to the ferromagnetism and superparamagnetism of small-sized, ferro- and ferrimagnetic iron oxide nanoparticles in the magnetic NC hybrid nanomaterials [20]. It was also shown that the saturation magnetization values of the magnetic NC composites can be connected to the changes in the surface of the NC [18]. Also, superparamagnetic-like behavior was observed when iron-oxide nanoparticles were embedded in sodium carboxymethyl cellulose (Na-CMC) [25], or within core–shell structure of β -cyclodextrin-modified cellulose crystals, CNC@Fe₃O₄@SiO₂ [26]. The use of the core-shell nanomaterials, Fe₃O₄-based layered nanostructures in bio-sensor application is discussed in literature [27]. It was shown that nanomaterials in show advantages in bio-sensor efficiency due to high surface/volume ratio, rapid reaction and lower threshold. MNP-Au was used for sandwich immunoassay, which could be easily handled by magnetic field. This approach gives a huge potential for application of MNP based composites in biosensors. Moreover, oxidized microcrystalline cellulose may form complex with Fe2+ ions, which can be used as reinforcement inside the composite materials. As a result, these materials are utilized in the area of magnetographic printing and security paper production [28]. It is important to notice that there are a number of parameters that influence magnetic response and its potential impact on electrical and/or multiferroic properties of the NC/Fe₃O₄ hybrid materials. For numerous applications, it is especially important to determine and correlate the structural and morphological properties with bond parameters, as well as magnetic interactions, by calculation exchange coupling constants, in hybrid materials. Unfortunately, there are not many reports in the literature that use density functional theory DFT in order to describe the interactions in cellulose based composites [29]. Moreover, to the best of the authors' knowledge, DFT calculation hasn't been performed on NC/Fe₃O₄ composite, yet. These results could be of great importance for the sake of further development of multicomponent hybrid materials based on NC/Fe₃O₄.

Taking all this into account, the aim of this report is to analyze the influence of the different amounts of NC on the crystal structure and morphology of nanosized Fe₃O₄ functionalized NC composites. In order to enable further optimization of the magnetic

properties of these materials, theoretical calculation of magnetic interactions and magnetic couplings between iron atoms, within the investigated composites, was performed.

2. Materials and Methods

2.1. Materials

Commercially available cellulose was used for nanocellulose preparation. Components used for co-precipitation, FeSO₄ x 7H₂O and FeCl₃ x 6H₂O were purchased from Merck. Deionized water (DW), with resistivity of 18 M Ω cm, was used for NC washing, aqueous solution preparation and for dish washing.

2.2. Preparation of NC/Fe₃O₄

Nanocellulose (NC) was prepared by acid hydrolysis (H2SO4) of commercially available cellulose, according to established procedure [30]. Obtained NC was separated from liquid phase by centrifugation and washed with deionized water until pH reached the value of 5.5. Functionalized nanocellulose was prepared by co-precipitation of Fe(II) and Fe(III) ions in aqueous solution containing NC with ammonia. NC, 1.5 g, was added to 200 ml distilled water and stirred for 10 min. FeCl₃ x 6H₂O and SO₄ x 7H₂O were added to a mixture as a sources of ferro and ferri ions, maintaining ratio 2:1 and heated at 60 °C. Chemical precipitation was achieved by adding 8.0 M ammonia solution dropwise with vigorous stirring and at constant pH of 10. Precipitation was followed with changes of orange color suspension to a black precipitate. Different concentrations of NC were achieved by reducing or increasing amount of NC in aqueous solutions, while maintaining the same concentrations of Fe(II) and Fe(III) ions. After incubation for 4 h at 60 °C, the mixture was cooled to room temperature with stirring. The resulting NC/Fe₃O₄ particles were washed several times with distilled water and ethanol, and dried after that. The weight ratio of NC in Fe₃O₄/NC was 1:0.25 (Fe₃O₄/NC1), 1:0.5 (Fe₃O₄/NC2), 1:1 (Fe₃O₄/NC₄), 1:2 (Fe₃O₄/NC₈).

2.3. Characterization Techniques

X-ray diffraction (XRD) data were obtained using a BRUKER D8 ADVANCE with Vario 1 focusing primary monochromator (Cu $k_{\alpha 1}$ radiation, λ = 1.54059 Å). XRD patterns were obtained over the Bragg angle (2 θ) range of 10-50°.

Fourier-transform infrared (FTIR) spectra of NC/Fe₃O₄ samples were recorded in the transmission mode, within the region 400 i 4000 cm⁻¹, using a BOMEM (Hartmann & Braun) spectrometer with a resolution of 4 cm⁻¹.

Dispersion state of Fe₃O₄ on nanocellulose surface and morphology of final composite films has been investigated by scanning electron microscopy (SEM, model: JEOL JSM 6610LV).

For theoretical calculation of magnetic interactions and magnetic couplings between iron atoms in magnetite structure within investigated composite materials, we performed Density Functional Theory - Broken Symmetry [31–34] using B3LYP [35, 36] and OPBE [37] functionals and TZP basis set.

3. Results and Discussion

132133

134

127

135 136 137

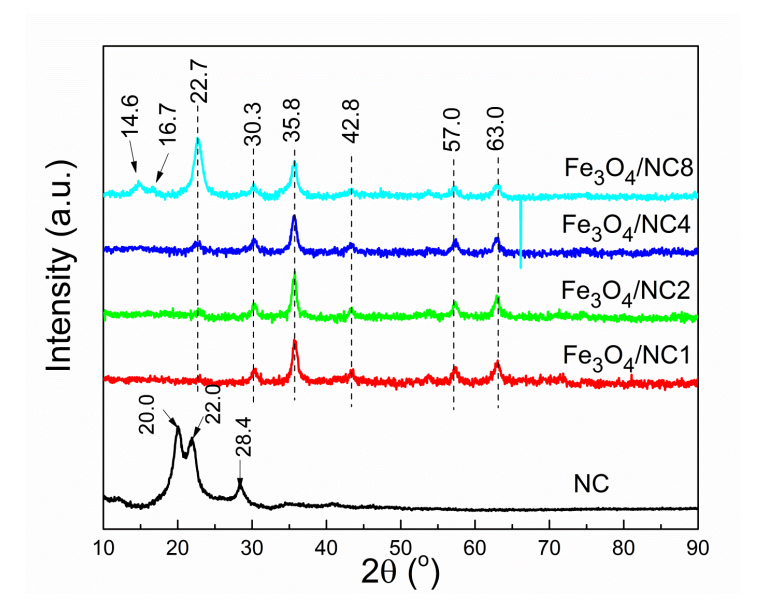


Figure 1. Diffractograms of NC and NC/Fe₃O₄ samples.

Changes in the crystal structure and phase purity, due to variation of NC loadings, are examined by diffraction of X-rays. The XRD diffractogram of the pure NC and the investigated Fe₃O₄/NC composite samples are shown in the Figure 1. The diffractogram of the pure NC shows typical cellulose II structure, with low intensity peak at 12° and strong doublet 20 and 22° [38,39]. Similar behavior was obtained by Lani at al. in [40], after acid hydrolysis of cellulose isolated from fruit bunch. With precipitation of Fe₃O₄ in alkali the conversion of cellulose II into cellulose I occurs. The characteristic signals at 30.3°, 35.8°, 42.8°, 57° and 63° suggest the presence of pure Fe₃O₄ with spinel structure [41] in Fe₃O₄/NC composites. Peak intensities of magnetite slightly decrease with increase in NC content, due to decrease of its concentration. The signals corresponding to cellulose are barely noticeable at Fe₃O₄/NC ratios of 1:0.25 and 1:0.5, and slightly increase when content of NC become equal to content of Fe₃O₄. Finally, at Fe₃O₄/NC 1:2 ratio, it becomes the most dominant peak in the graph. It was observed that signal corresponding to cellulose is slightly shifted from 22.0 to 22.7° in diffractograms of Fe₃O₄/NC, probably due to coupling of NC with magnetite nanoparticles.

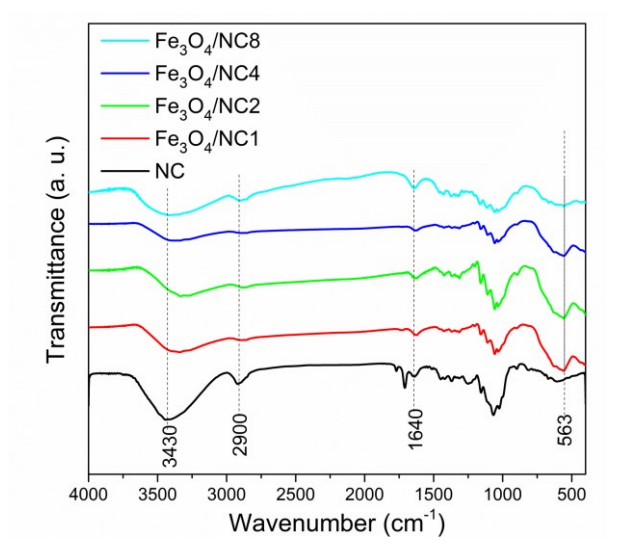


Figure 2. FTIR spectra of of Fe₃O₄/NC composites.

175

176

177

178

179

180

181

182

183

185 186

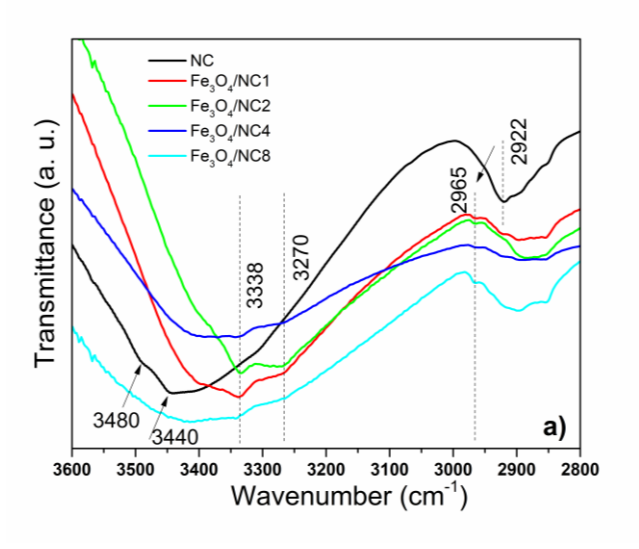
187

188

189

190

Fourier-transform infrared (FT-IR) spectroscopy in transmission mode was employed to investigate the variation in the infrared optical properties of NC with precipitation of Fe₃O₄ on the nanocellulose surface. The FT-IR transmittance spectra of NC and composite samples are shown in the Figure 2. The FTIR spectrum of pure nanocellulose was explained in detail in our previous publication [42]. In the spectra of magnetite/NC composites (Figure 2.), the bands originating from nanocellulose are the most dominant bands. Characteristic bands, assigned to O-H stretching vibration at 3430 cm⁻¹, C-H stretching vibrations of the -CH2 group at 2900 cm⁻¹ and -OH bending vibration at 1640 cm⁻¹, are observed in the spectra of all samples. High intensity broad band at around 563 cm⁻¹ is characteristic band of Fe-O in the tetrahedral sites [43]. Normally, this band appears at around 600 cm⁻¹ or little below this value, as suggested by literature [44]. Shift of this band to lower wave number is due to occurrence of Fe-O bonds on the surface of the nanocellulose. The decrease in the intensity of this signal is caused by lowering of Fe₃O₄ concentration, from sample Fe₃O₄/NC1 to Fe₃O₄/NC8, respectively. The shift of the O-H peak after deposition of Fe₃O₄ on the NC surface suggests the existence of interaction between the cellulose and magnetic nanoparticles [45].



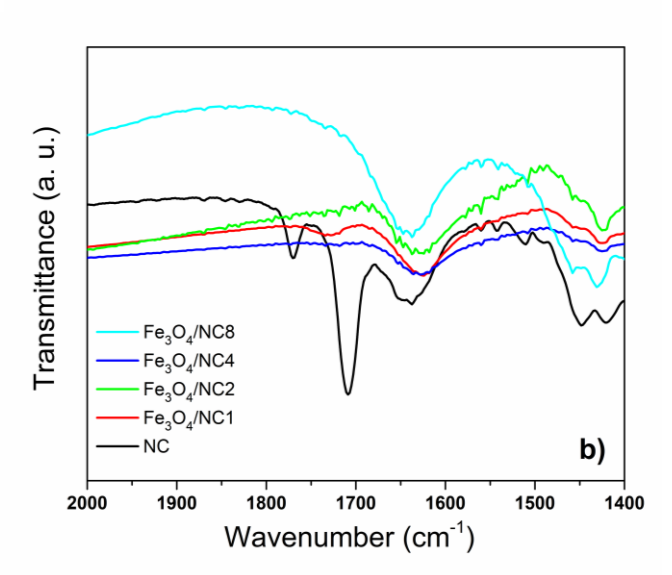


Figure 3. FTIR spectra of the NC and all modified samples a) 3600-2800 cm⁻¹ wavenumber range and b) 2000-1400 cm⁻¹ wavenumber range.

Region between 3600 and 2800 cm⁻¹ was additionally investigated and depicted in Figure 3 a). The maximum absorbance of the OH stretching vibration is positioned at 3440 cm⁻¹, indicating intramolecular hydrogen bonding of O2-H---O6 for CN sample. In the cases of the modified samples, O3-H---O5 and O6-H---O3 intramolecular hydrogen bonding were detected at 3338 cm⁻¹ and 3270 cm⁻¹, respectively [43]. It was observed that sample marked as NC exhibits typical cellulose II structure with low intensity band at 3480 cm⁻¹ and strong band at 3440 cm⁻¹. These bands are characteristic of cellulose II allomorph, and as it can be noticed from Figure 3 a), these bands were not detected in FTIR spectra of the samples modified with Fe₃O₄ nanoparticles. In the spectra of the hybrid materials (Fe₃O₄/NC1, Fe₃O₄/NC2, Fe₃O₄/NC4 and Fe₃O₄/NC8), bands at 3338 and 3270 cm⁻¹ were observed, indicating transition from cellulose II to cellulose I allomorph, which is in agreement with results obtained by XRD analysis. Further, the band at 1922 cm⁻¹ was significantly shifted to a higher wavenumber after addition of magnetic particles into the structure, suggesting exchange in the arrangements caused by changes of angles around β -1, 4-D-glycosidic linkages rearrangement [44].

 In the spectra showed in Figure 3 b), there are few obvious differences between NC and modified NC. First of all, the bands at 1720 cm⁻¹ and 1510 cm⁻¹, which are present in spectrum of pure nanocellulose, disappear in spectra of modified hybrid material. According to literature, these bands originate from C=C stretching vibration of the aromatic ring and the C=O stretching vibration of carboxylic groups of the lignin and hemicellulose [45]. It was shown earlier that these bands can despair after the treatment of cellulose with NaOH [46]. We have also used alkali environment during modification of nanocellulose with magnetic particles and we consider that as a reason for disappearance of earlier mentioned bands.

Shift to lower wavenumbers and broadening of the FTIR bands usually appear due to a presence of hydrogen bonds between cellulose and filler particles [47]. It was noticed that after introduction of Fe₃O₄ particles, bands of hydroxyl and carboxyl groups were downshifted, indicating formation of the hydrogen bonds among NC and the Fe₃O₄. Shift of the bands at 1640 cm⁻¹ and 1420 cm⁻¹ was detected in the spectra presented in Figure 3 b). With increasing amount of NC, the shift becomes smaller, and for the sample Fe₃O₄/NC8 this shift is almost indistinguishable. This indicates that lower number of hydrogen bonds between NC and the Fe₃O₄ was formed with decreasing percentage of magnetic nanoparticles in composites.

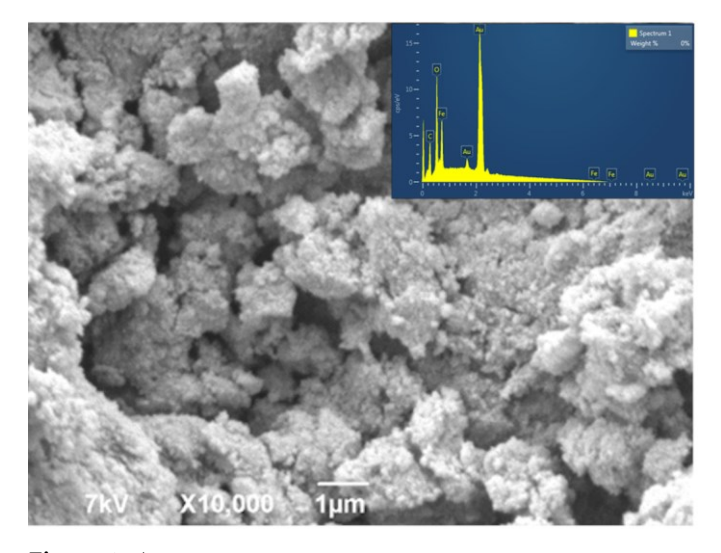


Figure 4. a).

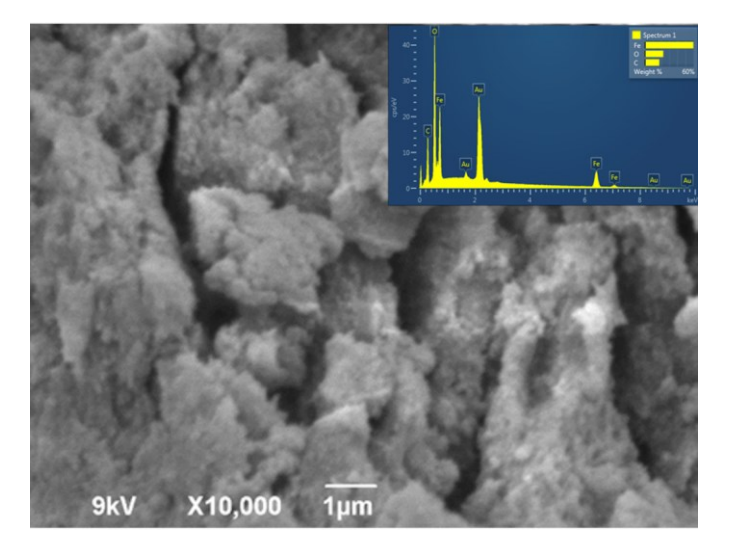


Figure 4. b).

218 219

220

221

217

223224225226227

228229230231232233

234

235236

10kV X10,000 1μm

Figure 4. c).

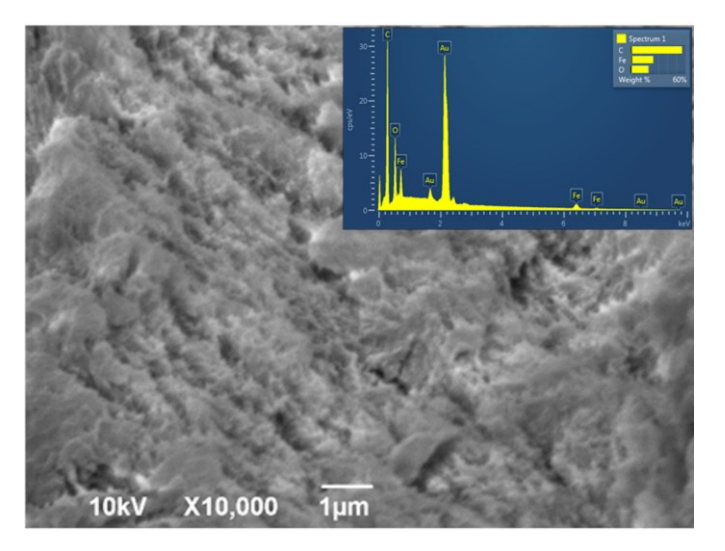


Figure 4. d).

Figure 4. SEM micrographs and EDS of the samples Fe3O4/NC whit different content of NC a) Fe3O4/NC1, b) Fe3O4/NC2, c) Fe3O4/NC4 and d) Fe3O4/NC8.

In addition, SEM analysis was used for morphological investigation of Fe₃O₄/NC (Figure 4). SEM micrographs indicate that lower amount of NC resulted in an aggregation and formation of agglomerates of magnetite particles, different in size and shape (Figure 4 a-c). The irregular Fe₃O₄ crystallites grew larger with lower loadings of NC in composite sample. Apparently, higher amount of NC favors more uniform deposition of Fe₃O₄ nanoparticles. The homogeneous deposition of Fe₃O₄ on the surface of nanocellulose was found for the sample with the highest content of NC (Figure 4d). Generally, it seems that nanocellulose high surface area plays a crucial role in their merging into homogeneous layer-like structures.

Energy dispersive X-ray analysis (EDS) was performed at the all Fe₃O₄/NC composite samples. The results confirmed the presence of Fe, C and O in the elemental compositions.

Improvement in homogeneity of the prepared sample continues with an increase in NC content (Fe₃O₄/NC4), i.e. availability of its larger surface area. Within Fe₃O₄/NC8 sample the higher substrate area lead to equal distribution of magnetite nanoparticles on NC surface.

Cellulose fibers modified by paramagnetic elements (deposition of iron) may enable improvement in cellulose orientation in a polymer matrix when exposed to lower strength

electric and magnetic fields [25]. Having in mind significant influence of the NC functionalization with Fe₃O₄ and its influence on magnetic properties of such materials, magnetic interactions in investigated magnetite structures were analyzed by determination of exchange coupling constants between neighboring iron atoms. Exchange couplings are described with the model of spin Hamiltonian, namely Heisenberg-Dirac-van Vleck (HDVV) Hamiltonian [48,49]which can be expressed by the Equation (1):

$$\hat{H}_{EX} = -J\hat{S}_A\hat{S}_B \tag{1}$$

where \widehat{S}_A and \widehat{S}_B stand for the effective spin operators, and J represents the exchange coupling constant. For the ferromagnetic interactions, with the parallel spin orientation, J has positive sign, while the negative sign indicates the antiferromagnetic interactions with antiparallel spin alignment.

The effective spin operators are related to the total spin operator (Equation (2))

$$\hat{\vec{S}} = \hat{\vec{S}}_A + \hat{\vec{S}}_B \tag{2}$$

Using the previous two equations, one can rewrite the Heisenberg–Dirac–Van Vleck Hamiltonian in the final form (Equation (3))

$$\hat{H}_{EX} = -\frac{J}{2} \left(\hat{\vec{S}}^2 - \hat{\vec{S}}_A^2 - \hat{\vec{S}}_B^2 \right) \tag{3}$$

Hence, the expression for the eigenvalues of H_{EX} for different spin states is presented in Equation (4).

$$E(^{2S+1}\Psi) = -\frac{J}{2}[S(S+1) - S_A(S_A+1) - S_B(S_B+1)]$$
(4)

where S, S_A , and S_B are the quantum numbers associated with the spin operators, while E^{2S+1} represents the energy of a spin multiplet.

In order to determine magnetic couplings between iron atoms in investigated magnetite structure, we performed Density Functional Theory - Broken Symmetry (DFT-BS) method developed by Noodleman [28–31]. Exchange coupling constants were estimated according to the Yamaguchi approach (Equation (5)) [50, 51].

$$J = (E_{HS} - E_{BS}) / \langle S^2 \rangle_{HS} - \langle S^2 \rangle_{RS}$$
 (5)

where EHs is the energy of the high spin, EBs is the energy of the broken symmetry, while $\left\langle S^2 \right\rangle_{HS}$ and $\left\langle S^2 \right\rangle_{BS}$ are the expectation values of the high-spin and broken symmetry spin operators.

All calculations were done using B3LYP [32, 33] hybrid functional and TZP basis set. For comparison purposes, coupling constants were also calculated with the OPBE [34] functional. All calculations were performed with the ORCA program package, version 2.8-20 [52].

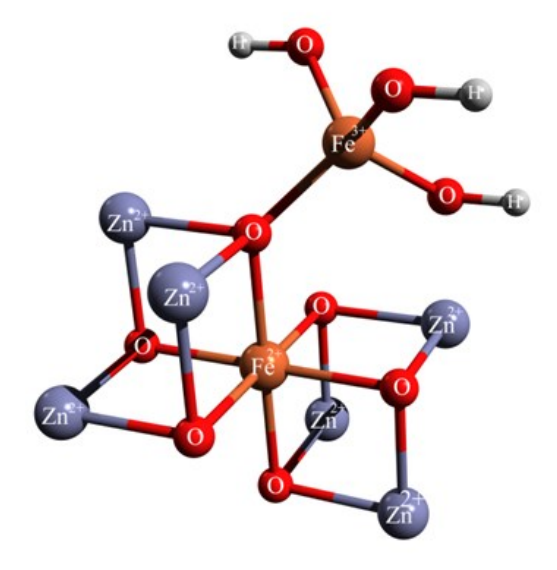


Figure 5. Structure of Fe3O4 model systems.

The exchange coupling constants between Fe^{2+} and Fe^{3+} ions were calculated on Fe_3O_4 model systems in which the first coordination sphere around iron atoms was taken directly from the crystal structures (Figure 5.). The other atoms were replaced with zinc ions and hydrogen atoms. This represents very useful method for calculation of exchange coupling constants in polynuclear metal complexes.

Calculated exchange coupling constants, as well as relevant bond distances, are presented in Table 1.

Table 1. Calculated exchange coupling constants (cm⁻¹) at OPBE and B3LYP level of theory and relevant bond distances (Å) from X-ray data.

Structure	Јорве	J _{B3LYP}	Fe ²⁺ -O	Fe ³⁺ -O
Fe ₃ O ₄ /NC1	48.7	46.7	2.081	1.846
Fe ₃ O ₄ /NC2	49.8	48.1	2.069	1.835
Fe ₃ O ₄ /NC4	49.3	47.7	2.073	1.839
Fe ₃ O ₄ /NC8	49.5	47.8	2.071	1.837

In all cases predominant ferromagnetic coupling was obtained. Although B3LYP functional represents the method of choice for the calculation of exchange coupling constants, the results obtained with the OPBE functional are quite similar. Calculated values are slightly lower at B3LYP level of theory, in comparison to OPBE level of theory. Ferromagnetic interactions are the consequence of electronic structure and coordination environment around metal ions. The coordination around Fe³⁺ is tetrahedral with high spin e(2)t₂(3) electronic configuration, while the Fe²⁺ ions have octahedral coordination with high spin t_{2g}(4)e_g(2) electronic configuration. Due to such coordination and orientation in space, the magnetic orbitals are spatially orthogonal, which leads to net ferromagnetic interactions.

It is well known that magnetic interactions between paramagnetic centers strongly depend on geometrical parameters, namely – on bond distances and angles. In most cases, magnetic interactions decrease with increasing bond distances and angles. The change in percentage of NC doesn't influence drastically change of Fe²+-O and Fe³+-O bond distances (Table 1.). Hence, the differences in magnetic couplings between Fe²+ and Fe³+ ions in investigated structures are very small and show weak dependence to the percentage of NC. In the case of Fe₃O₄/NC1 sample, the Fe²+-O and Fe³+-O bond distances are slightly longer in comparison to other structures, i.e. 2.081 and 1.846 Å respectively. Indeed, ferromagnetic interactions in such case are slightly lower.

296

297

298

299

300 301

302

303

304

305 306

307

309

310

311

312

313

314

315

316 317

318

319

320 321

322

323 324

325

326 327

328 329

330

331 332

333 334

335

337

338 339

340

341

342

343

344 345

346

4. Conclusion

In this study the investigation of the influence of nanocellulose amount on features of hybrid composite materials based on functionalized nanocellulose with magnetic particles has been presented. We were focused on the investigation of the structural and morphological properties of nanocellulose/magnetite (Fe₃O₄/NC) composites. XRD analysis confirmed transformation from cellulose II into cellulose I allomorph with addition of magnetic particle. Further, small but noticeable shift of diffraction line at Bragg angle of 22º indicates coupling between phases. Detailed FTIR analysis confirmed results obtained by XRD, i.e. transition among allomorph along with changes in structure due to covering of NC with Fe₃O₄. In order to enable further development of multicomponent hybrid materials based on NC/Fe₃O₄, theoretical calculation of magnetic interactions and magnetic couplings between iron atoms in magnetite structure within investigated composite materials were performed. B3LYP hybrid functional and TZP basis set were used for calculation of bond distances and for determination of coupling constants between neighboring iron atoms in Fe₃O₄/NC composites. The derived model confirmed predominant ferromagnetic coupling. It was shown that amount of NC has influence on bounds distance and angles. This conclusion suggests that NC content may affect magnetic couplings between neighboring Fe³⁺ and Fe²⁺ ions.

Funding: This work is supported by the Ministry of Education, Science and Technological Development of Republic of Serbia under the Projects 451-03-68/2020-14/200175, 451-03-9/2021-14/200116, 451-03-9/2021-14/200105, 451-03-9/2021-14/200017 and USA NSF PREM award DMR 11523617.

Author Contributions: Aleksandra Janićijevic: Writing - Original Draft, Investigation; Vera P. Pavlovic: Formal analysis, Writing - Review & Editing, Visualization; Danijela Kovacevic: Resources, Investigation; Marko Peric: Software; Branislav Vlahovic: Writing - Review & Editing, Supervision, Methodology; Vladimir B. Pavlovic: Writing - Review & Editing, Supervision, Methodology, Project administration; Suzana Filipovic: Writing - Review & Editing, Supervision, Visualization.

Data availability: The raw/processed data required to reproduce these findings cannot be shared at this time as the data also forms part of an ongoing study.

References

- 1. Rejab, M.R.B.M.; Hamdan, M.H.B.M.; Quanjin, M.; Siregar, J.P.; Bachtiar, D.; Muchlis, Y. Historical Development of Hybrid Materials, in: *Encyclopedia of Renewable and Sustainable Materials, Elsevier* **2020**, 445–455.
- 2. Gu, H.; Liu, C.; Zhu, J.; Gu, J.; Wujcik, E.K.; Shao, L.; Wang, N.; Wei, H.; Scaffaro, R.; Zhang, J.; Guo, Z. Introducing advanced composites and hybrid materials, *Adv Compos Hybrid Mater.* **2018**, 1, 1–5.
- 3. Ashby, M.F. Hybrids to fill holes in material property space, *Philosophical Magazine* **2005**, *85*, 3235–3257.
- 4. Kumar, J.; Singh, R.K.; Samanta, S.B.; Rastogi, R.C.; Singh, R. Single-step magnetic patterning of iron nanoparticles in a semiconducting polymer matrix, *Macromolecular Chemistry and Physics* **2006**, 207, 1584–1588.
- 5. Gonçalves, R.; Martins, P.M.; Caparrós, C.; Martins, P.; Benelmekki, M.; Botelho, G.; Lanceros-Mendez, S.; Lasheras, A.; Gutiérrez, J.; Barandiarán, J.M. Nucleation of the electroactive b-phase, dielectric and magnetic response of poly(vinylidene fluoride) composites with Fe₂O₃ nanoparticles, *J of Non-Crystalline Solids* **2013**, *361*, 93–99.
- 6. Jayakumar, O.D.; Mandal, B.P.; Majeed, J.; Lawes, G.; Naik, R.; Tyagi, K. Inorganic-organic multiferroic hybrid films of Fe₃O₄ and PVDF with significant magneto-dielectric coupling, *J Mater Chem C* **2013**, *1*, 3710–3715.
- 7. Shabanian, M.; Khoobi, M.; Hemati, F.; Khonakdar, H.A.; Esmaeil S.; Ebrahimi, S.; Wagenknecht, U.; Shafiee, A. New PLA/PEI-functionalized Fe₃O₄ nanocomposite: Preparation and characterization, *J Industrial Eng Chem* **2015**, 24, 211–218.
- 8. Huo, X.; Li, W.; Zhu, J.; Li, L.; Li, Y.; Luo, L.; Zhu, Y. Composite Based on Fe₃O₄@BaTiO₃ Particles and Polyvinylidene Fluoride with Excellent Dielectric Properties and High Energy Density, *J Phys Chem C* **2015**, *119*, 25786–25791.
- 9. Tsonos, C.; Soin, N.; Tomara, G.; Yang, B.; Psarras, G.C.; Kanapitsas, A.; Siores, E. Electromagnetic wave absorption properties of ternary poly(vinylidene fluoride)/magnetite nanocomposites with carbon nanotubes and graphene, *RSC Advances* **2016**, *6*, 1919–1924.
- 10. Gu, H.; Zhou, X.; Lyu, S.; Pan, D.; Dong, M.; Wu, S.; Ding, T.; Wei, X.; Seok, I.; Wei, S.; Guo, Z. Magnetic nanocellulose-magnetite aerogel for easy oil adsorption, *J Colloid Interf Sci* **2020**, *560*, 849–856.
- 11. Amiralian, N.; Mustapic, M.; Hossain, Md.S.A.; Wang, C.; Konarova, M.; Tang, J.; Na, J.; Khan, A.; Rowan, A. Magnetic nanocellulose: A potential material for removal of dye from water, *J Hazard Mater* **2020**, *394*, 122571.

- 347 12. Shak, K.P.Y.; Pang, Y.L.; Mah, S.K. Nanocellulose: Recent advances and its prospects in environmental remediation, 348 *Beilstein J. Nanotech* **2018**, 924, 79–2498.
- 13. Anirudhan, T.S.; Rejeena, S.R. Aminated *β*-Cyclodextrin-Modified-Carboxylated Magnetic Cobalt/Nanocellulose Composite for Tumor-Targeted Gene Delivery, *J Appl Chem* **2014**, 2014, 1–10.
 - 14. Hernández-Flores, J.A.; Morales-Cepeda, A.B.; Castro-Guerrero, C.F.; Delgado-Arroyo, F.; Díaz-Guillén, M.R.; Cruz-Soto, J. de la; Magallón-Cacho, L.; León-Silva, U. Morphological and Electrical Properties of Nanocellulose Compounds and Its Application on Capacitor Assembly, *I J of Poly Sci* **2020**, 2020, e1891064.
 - 15. Tuukkanen, S.; Rajala, S. Nanocellulose as a Piezoelectric Material, Piezoelectricity Organic and Inorganic Materials and Applications. 1st ed. Intech Open, England, London, **2018**.
 - 16. El-Nahas, A.M.; Salaheldin, T.A.; Zaki, T.; El-Maghrabi, H.H.; Marie, A.M.; Morsy, S.M.; Allam, N.K. Functionalized cellulose-magnetite nanocomposite catalysts for efficient biodiesel production, *Chem Eng J* **2017**, 322, 167–180. https://doi.org/10.1016/j.cej.2017.04.031.
 - 17. Trache, D.; Tarchoun, A.F.; Derradji, M.; Hamidon, T.S.; Masruchin, N.; Brosse, N.; Hussin M.H., Nanocellulose: From Fundamentals to Advanced Applications, *Front Chem* **2020**, *8*, 329.
 - 18. Supramaniam, J.; Adnan, R.; Mohd Kaus, N.H.; Bushra, R. Magnetic nanocellulose alginate hydrogel beads as potential drug delivery system, *I J of Biolog Macromol* **2018**, *118*, 640–648.
 - 19. Li, W.; Zhao, X.; Liu, S. Preparation of entangled nanocellulose fibers from APMP and its magnetic functional property as matrix, *Carbohyd Polym* **2013**, *94*, 278–285.
 - 20. Nypelö, T.; Rodriguez-Abreu, C.; Kolen'ko, Y.V.; Rivas, J.; Rojas, O.J. Microbeads and Hollow Microcapsules Obtained by Self-Assembly of Pickering Magneto-Responsive Cellulose Nanocrystals, *ACS Appl. Mater. Interfaces.* **2014**, *6*, 16851–16858.
 - 21. Fujisawa, S.; Kaku, Y.; Kimura, S.; Saito, T. Magnetically Collectable Nanocellulose-Coated Polymer Microparticles by Emulsion Templating, *Langmui*. **2020**, *36*, 9235–9240.
 - 22. Taleb, K.; Markovski, J.; Veličković, Z.; Rusmirović, J.; Rančić, M.; Pavlović, V.; Marinković, A. Arsenic removal by magnetite-loaded amino modified nano/microcellulose adsorbents: Effect of functionalization and media size, *Arab J Chem* **2019**, *12*, 4675–4693.
 - 23. Luna-Martínez, J.F.; Reyes-Melo, E.; González-González, V.; Guerrero-Salazar, C.; Torres-Castro, A.; Sepúlveda-Guzmán, S. Synthesis and characterization of a magnetic hybrid material consisting of iron oxide in a carboxymethyl cellulose matrix, *J Appl Polym Sci* **2013**, 127, 2325–2331.
 - 24. Chen, L.; Berry, R.M.; Tam, K.C. Synthesis of β-Cyclodextrin-Modified Cellulose Nanocrystals (CNCs)@Fe₃O₄@SiO₂ Superparamagnetic Nanorods, *ACS Sustainable Chem. Eng* **2014**, *2*, 951–958.
 - 25. Sundar, S.T.; Sain, M.M.; Oksman, K. Characterization of microcrystalline cellulose and cellulose long fiber modified by iron salt, *Carbohyd Polym* **2010**, *80*, 35–43.
 - 26. Zarei, S.; Niad, M.; Raanaei, H. The removal of mercury ion pollution by using Fe₃O₄-nanocellulose: Synthesis, characterizations and DFT studies, *J Hazard Mater* **2018**, 344, 258-273.
 - 27. Bondeson, D.; Mathew, A.; Oksman, K. Optimization of the isolation of nanocrystals from microcrystalline cellulose by acid hydrolysis, *Cellulose* **2006**, *13*, 171–180.
 - 28. Noodleman, L.; Norman, J.G.; Osborne, J.H.; Aizman, A.; Case, D.A. Models for ferredoxins: electronic structures of iron-sulfur clusters with one, two, and four iron atoms, *J Am Chem Soc* **1985**, *107*, 3418–3426.
 - 29. Noodleman, L.; Case, D.A.; Aizman, A. Broken symmetry analysis of spin coupling in iron-sulfur clusters, *J Am Chem Soc* **1988**, *110*, 1001–1005.
 - 30. Noodleman, L.; Peng, C.Y.; Case, D.A.; Mouesca, J.-M. Orbital interactions, electron delocalization and spin coupling in iron-sulfur clusters, *Coord Chem Rev* **1995**, 144, 199–244.
 - 31. Noodleman, L. Valence bond description of antiferromagnetic coupling in transition metal dimers, *J Chem Phys* **1981**, *74*, 5737–5743.
 - 32. Becke, A.D. Density functional calculations of molecular bond energies, J Chem Phys 1986, 84, 4524–4529.
 - 33. Perdew, J.P.; Yue, W. Accurate and simple density functional for the electronic exchange energy: Generalized gradient approximation, *Phys Rev B* **1986**, 33, 8800–8802.
 - 34. Swart, M.; Ehlers, A.W.; Lammertsma, K. Performance of the OPBE exchange-correlation functional, *Mol Phys* **2004**, *102*, 2467–2474.
 - 35. Yue, Y. A comparative study of cellulose I and II and fibers and nanocrystals, LSU Master's Theses, 2011.
 - 36. Mansikkamäki, P.; Lahtinen, M.; Rissanen, K. Structural Changes of Cellulose Crystallites Induced by Mercerisation in Different Solvent Systems; Determined by Powder X-ray Diffraction Method, *Cellulose* **2005**, *12*, 233–242.
 - 37. Lani, N.S.; Ngadi, N.; Johari, A.; Jusoh, M. Isolation, Characterization, and Application of Nanocellulose from Oil Palm Empty Fruit Bunch Fiber as Nanocomposites, *J Nanomater* **2014**, 2014, e702538.
- 401 38. Anirudhan, T.S.; Rejeena, S.R. Poly(methacrylic acid-co-vinyl sulfonic acid)-grafted-magnetite/ nanocellulose super-402 absorbent composite for the selective recovery and separation of immunoglobulin from aqueous solutions, *Sep Purif Technol* **2013**, 119, 82–93.

407

408

409 410

411 412

413

414

415

416

417

418 419

420

421

422

423

424 425

426 427

- 39. Djordjevic, N.; Marinkovic, A.; Nikolic, J.; Drmanic, S.; Rancic, M.; Brkovic, D.; Uskokovic, P. A study of the barrier properties of polyethylene coated with nanocellulose/magnetite composite film, *J Serb Chem Soc.* **2016**, 81, 589–605.
 - 40. Nyquist, R.O.; Kagel, R. A. Infrared Spectra of Inorganic Compounds (3800–45 cm⁻¹), Academic Press, New York, **1971**.
 - 41. Anggraini Yossy, H.; Nanocomposites Comprising Cellulose and Nanomagnetite as Heterogeneous Catalysts for the Synthesis of Biodiesel from Oleic Acid, *I J Tech* **2019**, *10*, 798-807.
 - 42. Rusmirović, J.D.; Ivanović, J.Z.; Pavlović, V.B.; Rakić, V.M.; Rančić, M.P.; Djokić, V.; Marinković, A.D. Novel modified nanocellulose applicable as reinforcement in high-performance nanocomposites, *Carbohyd Polym* **2017**, *164*, 64–74.
 - 43. Oh, S.Y.; Yoo, D.I.; Shin, Y.; Seo, G. FTIR analysis of cellulose treated with sodium hydroxide and carbon dioxide, *Carbohyd Res* **2005**, *340*, 417–428.
 - 44. Liu, X.; Khor, S.; Petinakis, E.; Yu, L.; Simon, G.; Dean, K.; Bateman, S. Effects of hydrophilic fillers on the thermal degradation of poly(lactic acid), *Thermochim Acta* **2010**, *509*, 147–151.
 - 45. Wulandari, W.T.; Rochliadi, A.; Arcana I.M. Nanocellulose prepared by acid hydrolysis of isolated cellulose from sugarcane bagasse, *IOP Conf. Ser.: Mater. Sci. Eng* **2016**, *107*, 012045.
 - 46. Zheng, D.; Zhang, Y.; Guo, Y.; Yue, J. Isolation and Characterization of Nanocellulose with a Novel Shape from Walnut (Juglans Regia L.) Shell Agricultural Waste, *Polym* **2019**, *11*, 1130.
 - 47. Yu, Y.; Wang, Y.; Deng, P.; Zhang, T. Fe₃O₄@rGO hybrids intercalated nanocellulose-based aerogels for enhanced ferromagnetic and mechanical properties, *J App Polym Sci* **2020**, *137*, 48564.
 - 48. Heisenberg, W. Zur Theorie des Ferromagnetismus, Z. Physik 1928, 49, 619–636.
 - 49. Dirac, P.A.M. The Principles of Quantum Mechanics, Clarendon Press, Oxford, 1947.
 - 50. Soda, T.; Kitagawa, Y.; Onishi, T.; Takano, Y.; Shigeta, Y.; Nagao, H.; Yoshioka, Y.; Yamaguchi, K. Ab initio computations of effective exchange integrals for H–H, H–He–H and Mn₂O₂ complex: comparison of broken-symmetry approaches, *Chem Phys Lett* **2000**, *319*, 223–230.
 - 51. Yamaguchi, K.; Takahara, Y.; Fueno, T. Ab-Initio Molecular Orbital Studies of Structure and Reactivity of Transition Metal-OXO Compounds, in: V.H. Smith, H.F. Schaefer, K. Morokuma (Eds.), *Appl Quan Chem* **1986** 155–184.
- 52. Neese, F. ORCA An ab initio, DFT and semiempirical electronic structure package, version 2.8, revision 15, Max-Planck-Institute für Bioanorganische Chemi, 2009.